

Accepted Manuscript

(2E)-2-[1-(1,3-benzodioxol-5-yl)-3-(1*H*-imidazole-1-yl)propylidene]-*N*-(4-methoxyphenyl)hydrazinecarboxamide: Synthesis, crystal structure, vibrational analysis, DFT computations, molecular docking and antifungal activity

Reem I. Al-Wabli, Alwah R. Al-Ghamdi, I.P. Primsa, Hazem A. Ghabbour, Mohamed H. Al-Agamy, I. Hubert Joe, Mohamed I. Attia

PII: S0022-2860(18)30448-4

DOI: [10.1016/j.molstruc.2018.04.017](https://doi.org/10.1016/j.molstruc.2018.04.017)

Reference: MOLSTR 25090

To appear in: *Journal of Molecular Structure*

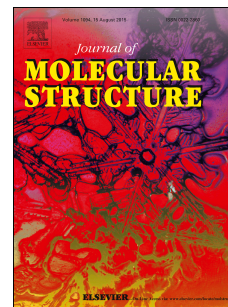
Received Date: 11 February 2018

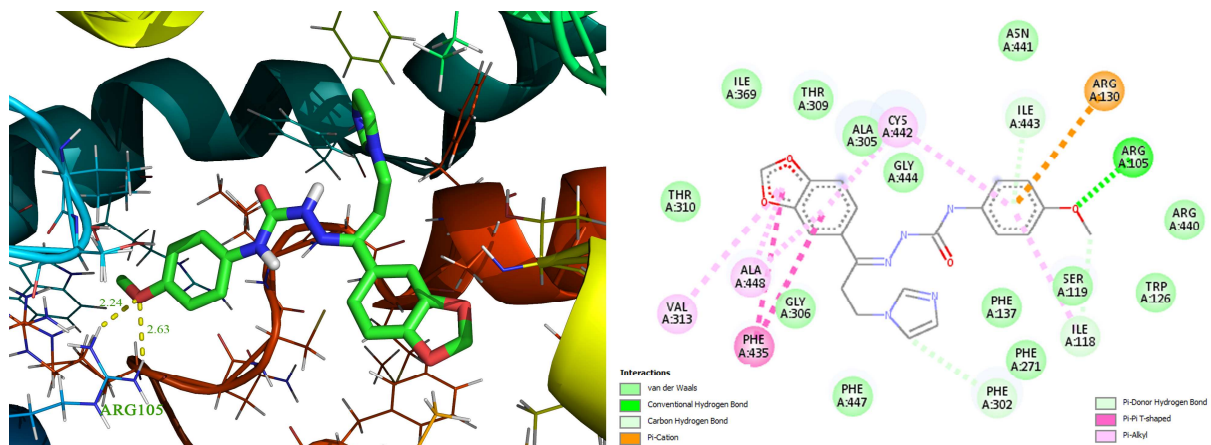
Revised Date: 3 April 2018

Accepted Date: 3 April 2018

Please cite this article as: R.I. Al-Wabli, A.R. Al-Ghamdi, I.P. Primsa, H.A. Ghabbour, M.H. Al-Agamy, I.H. Joe, M.I. Attia, (2E)-2-[1-(1,3-benzodioxol-5-yl)-3-(1*H*-imidazole-1-yl)propylidene]-*N*-(4-methoxyphenyl)hydrazinecarboxamide: Synthesis, crystal structure, vibrational analysis, DFT computations, molecular docking and antifungal activity, *Journal of Molecular Structure* (2018), doi: 10.1016/j.molstruc.2018.04.017.

This is a PDF file of an unedited manuscript that has been accepted for publication. As a service to our customers we are providing this early version of the manuscript. The manuscript will undergo copyediting, typesetting, and review of the resulting proof before it is published in its final form. Please note that during the production process errors may be discovered which could affect the content, and all legal disclaimers that apply to the journal pertain.





(2E)-2-[1-(1,3-Benzodioxol-5-yl)-3-(1H-imidazol-1-yl)propylidene]-N-(4-methoxyphenyl)hydrazinecarboxamide: Synthesis, crystal structure, vibrational analysis, DFT computations, molecular docking and antifungal activity

Reem I. Al-Wabli^a, Alwah R. Al-Ghamdi^a, I. P. Primsa^{b,c}, Hazem A. Ghabbour^{a,d}, Mohamed H. Al-Agamy^{e,f}, I. Hubert Joe^b and Mohamed I. Attia^{a,g*}

^aDepartment of Pharmaceutical Chemistry, College of Pharmacy, King Saud University, P.O. Box 2457, Riyadh 11451, Saudi Arabia

^bCentre for Molecular and Biophysics Research, Department of Physics, Mar Ivanios College, Thiruvananthapuram 695 015, Kerala, India

^cDepartment of Physics, Sree Narayana College, Sivagiri, Varkala, Thiruvananthapuram 695 145, Kerala, India

^dDepartment of Medicinal Chemistry, Faculty of Pharmacy, Mansoura University, Mansoura 35516, Egypt

^eDepartment of Pharmaceutics, College of Pharmacy, King Saud University, P.O. Box 2457, Riyadh 11451, Saudi Arabia

^fMicrobiology and Immunology Department, Faculty of Pharmacy, Al-Azhar University, Cairo 11884, Egypt

^gMedicinal and Pharmaceutical Chemistry Department, Pharmaceutical and Drug Industries Research Division, National Research Centre (ID: 60014618), El Bohooth Street, Dokki, Giza 12622, Egypt

Keywords: Synthesis; Crystal structure; Imidazole; Antifungal; DFT

Abstract

Fungal infections are a growing health threat to mankind. The development of novel potent antifungal agents is a challenge to overcome the resistance to the available antifungal medications. The current report focuses on the synthesis and spectroscopic characterisation of a new imidazole-bearing antifungal agent. The vibrational characteristics of the title compound are explored using Fourier transform infrared and Raman spectroscopy with the aid of density functional theory. Highest occupied and lowest unoccupied molecular orbital investigations and natural bond orbital analysis of the title molecule are performed to investigate the possible intermolecular delocalisation or hyper-conjugation, and the possible interactions with the target protein. Single crystal X-ray analysis confirms the assigned (*E*)-configuration of the imine double bond structure of the title compound. The molecular structure of the title compound is crystallised in a monoclinic space group, namely, $P2_1/c$, $a = 10.7007(4) \text{ \AA}$, $b = 7.3072(3) \text{ \AA}$, $c = 24.9088(8) \text{ \AA}$, $\beta = 97.178(2)^\circ$, $V = 1932.41(12) \text{ \AA}^3$ and $Z = 4$. The antifungal potential of the title compound is *in vitro* assessed against four fungal strains. In addition, molecular docking of the title molecule predicts its binding orientation in the active site of the target protein.

1. Introduction

Global morbidity due to life-threatening fungal infections has dramatically increased in recent decades, particularly among individuals suffering from cancer, autoimmune diseases, organ transplants or AIDS [1-3]. *Candida albicans* is a leading cause for ~70% of fungal infections in humans [4]. The emergence of drug resistance to the currently available antifungal medications has become the key focus of many researchers and pharmaceutical companies, motivating them to develop novel antifungal agents capable of overcoming this resistance, as well as possessing potent activity, low toxicity and a broad spectrum of activity [5].

During the past 35 years, azole compounds bearing either imidazole or triazole pharmacophore moieties have been the most widely used antifungal drugs and have had a substantial impact on the management of systemic fungal infections [6]. Azoles are an important class of antifungal chemotherapeutic agents that prevent the biosynthesis of ergosterol by inhibiting cytochrome P450-dependent sterol 14 α -demethylase enzyme [7, 8].

Alternatively, literature screening exposed that a number of compounds bearing the semicarbazone fragment in their chemical structure exhibit significant antifungal and antibacterial activities [9, 10]. In addition, a plethora of bioactive molecules incorporate the 1,3-benzodioxole scaffold in their structure [11-13].

It was on this basis that the title compound, namely, (2*E*)-2-[1-(1,3-benzodioxol-5-yl)-3-(1*H*-imidazol-1-yl)propylidene]-*N*-(4-methoxyphenyl)hydrazine carboxamide, was designed and synthesised as a molecular hybrid incorporating the imidazole pharmacophore, as well as semicarbazone and 1,3-benzodioxole fragments. The assigned chemical structure of the title compound was determined with different spectroscopic techniques and the configuration of its imine double bond was unambiguously proved *via* single crystal X-ray analysis. The antifungal potential of the title molecule was assessed using a minimum inhibitory concentration (MIC) assay towards four fungal strains. Furthermore, a detailed vibrational spectral analysis was conducted with the aid of density functional theory (DFT) computations in order to gain insight into the inter- and intramolecular interactions of the title compound. Natural bond orbital (NBO) analysis of the title molecule was performed to determine the possible intermolecular delocalisation or hyperconjugation, while HOMO-LUMO investigations explored the possible interactions between the title compound and its target protein. A molecular docking study predicted the binding pose of the title compound to its target protein.

2. Experimental details

2.1. General

The FT-IR spectrum of the title compound was recorded using a Perkin-Elmer RXL spectrophotometer in the region of 4000–400 cm⁻¹, with samples in the KBr pellet method with a resolution of 2 cm⁻¹. The Raman spectrum was recorded in the region of 3500–50 cm⁻¹ using a Bruker RFS 27 standalone FT-Raman spectrometer with a resolution of 2 cm⁻¹.

2.2. Synthesis

A reaction mixture containing *N*-(4-methoxyphenyl)hydrazinecarboxamide [14] (1.81 g, 10 mmol), ketone **3** [15] (0.24 g, 10 mmol) and a few drops of glacial acetic acid in absolute ethanol (15 mL) was stirred at room temperature for 18 h. The reaction mixture was evaporated under reduced pressure and the residue was purified by recrystallisation from ethanol to furnish the title semicarbazone **4**. Yield 0.51 g (51%); white powder m.p. 161–163 °C; ¹H-NMR (DMSO-*d*₆): δ (ppm) 3.26 (t, *J* = 6.5 Hz, 2H, –CH₂–CH₂–N), 3.75 (s, 3H, OCH₃), 4.09 (t, *J* = 6.5 Hz, 2H, –CH₂–CH₂–N), 6.07 (s, 2H, –O–CH₂–O–), 6.86 (s, 1H, –N–CH=CH–N=), 6.89 (d, *J* = 2.0 Hz, 1H, Ar–H), 6.91 (s, 2H, Ar–H), 7.26 (dd, *J* = 1.5, 8.5 Hz, 1H, Ar–H), 7.28 (s, 1H, –N–CH=CH–N=), 7.51 (d, *J* = 8.5 Hz, 2H, Ar–H), 7.64 (br.s, 2H, Ar–H, –N–CH=N–), 8.77 (s, 1H, NH), 10.05 (s, 1H, NH); ¹³C-NMR (DMSO-*d*₆): δ(ppm) 28.6 (–CH₂–CH₂–N), 42.7 (–CH₂–CH₂–N), 55.7 (OCH₃), 101.7 (–O–CH₂–O–), 107.2, 108.2, 114.1 (Ar–CH), 119.9 (–N–CH=CH–N=), 121.2, 122.9, 128.7, 131.7, 132.4 (Ar–CH, Ar–C, –

N-CH=CH-N=), 137.8 (-N-CH=N-), 144.9, 148.2, 148.4, 154.4, 155.6 (Ar-C, C=O, C=N); MS m/z (ESI): 408.1 [M + H]⁺, 430.1 [M + 23]⁺, 446.1 [M + 39]⁺.

2.3. X-ray analysis

The title compound was obtained as single crystals by slow evaporation of an ethanolic solution of the pure compound at room temperature. Data were collected on a Bruker APEX-II D8 Venture area diffractometer, equipped with graphite monochromatic Cu $K\alpha$ radiation, $\lambda = 1.54178 \text{ \AA}$ at 296 (2) K. Cell refinement and data reduction were carried out by Bruker SAINT. SHELXT [16, 17] was used to solve the structure. The final refinement was carried out by full-matrix least-squares techniques with anisotropic thermal data for non-hydrogen atoms. The crystallographic data and refinement information of the title compound, C₂₁H₂₁N₅O₄, are summarised in Table 1. CCDC 1555563 contains the supplementary crystallographic data for this compound and can be obtained free of charge from the Cambridge Crystallographic Data Centre *via* www.ccdc.cam.ac.uk/data_request/cif.

Table 1. Experimental X-ray details of the title compound.

Crystal data	
Chemical formula	C ₂₁ H ₂₁ N ₅ O ₄
Mr	407.43
Crystal system, space group	Monoclinic, $P2_1/c$
Temperature (K)	296
a, b, c (Å)	10.7007 (4), 7.3072 (3), 24.9088 (8)
β (°)	97.178 (2)
V (Å ³)	1932.41 (12)
Z	4
Radiation type	Cu $K\alpha$
μ (mm ⁻¹)	0.82
Crystal size (mm)	0.36 × 0.15 × 0.11
Data collection	
Diffractometer	Bruker APEX-II D8 venture diffractometer
Absorption correction	Multi-scanSADABS Bruker 2014
Tmin, Tmax	0.757, 0.913
No. of measured, independent and observed [$I > 2\sigma(I)$] reflections	9324, 3380, 2388
R_{int}	0.039
Refinement	
$R[F^2 > 2\sigma(F^2)]$, $wR(F^2)$, S	0.049, 0.132, 1.06
No. of reflections	3380
No. of parameters	280
No. of restraints	0
H-atom treatment	H atoms treated by a mixture of independent and constrained refinement
$\Delta\rho_{\text{max}}$, $\Delta\rho_{\text{min}}$ (e Å ⁻³)	0.22, -0.23

2.4. Computational techniques

Quantum chemical calculations were conducted using the Gaussian '09 program package [18] with the B3LYP/6-311++G(d,p) basis set [19, 20]. The vibrational frequencies were scaled by a factor of 0.9673 to compensate for the errors due to vibrational anharmonicities and the incompleteness of the basis set [21]. Vibrational wavenumbers were assigned by potential energy distribution analysis using the VEDA 4 program [22]. NBO analysis was performed by NBO the 3.1 program [23]. The molecular docking analysis was carried out using the AutoDock 4.2 program [24].

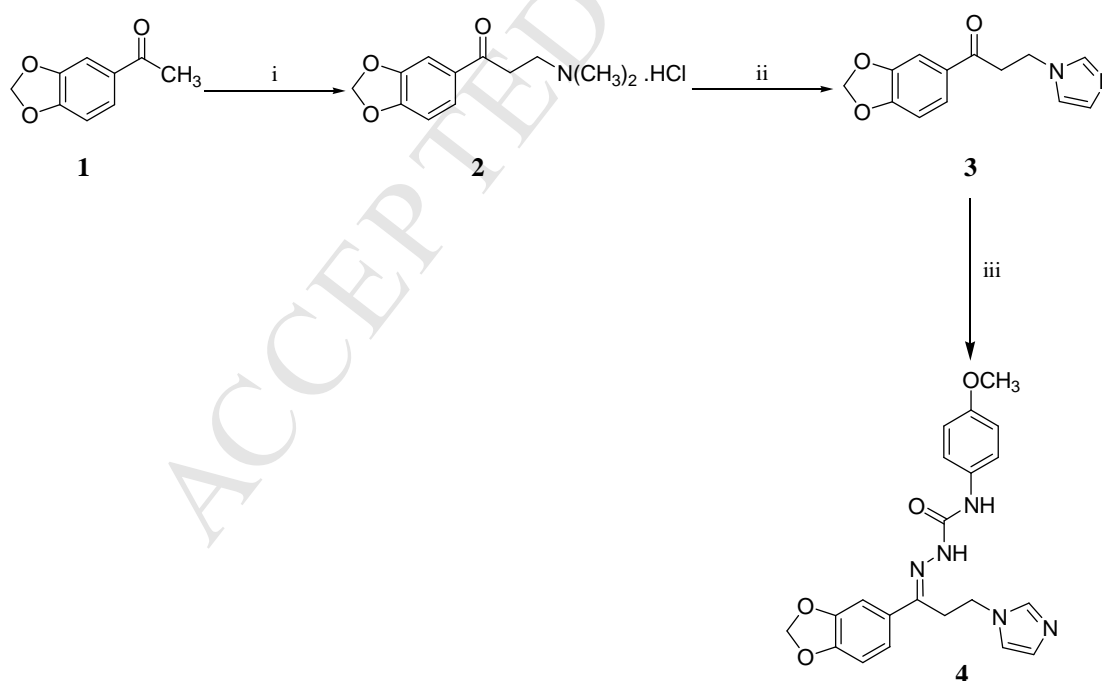
2.5. Antifungal activity

Fungal inocula were prepared as reported in the literature [15] and the MIC values of the title compound were determined as previously reported [15].

3. Results and discussion

3.1. Synthesis

The title compound **4** was prepared as illustrated in Scheme 1. Thus, the commercially available acetophenone derivative **1** was subjected to Mannich reaction to furnish the Mannich base hydrochloride **2** which was subsequently elaborated to the corresponding imidazole derivative **3**. Compound **3** was allowed to react with *N*-(4-methoxyphenyl)hydrazinecarboxamide to give the title compound **4**.



Reagents and conditions: i) HN(CH₃)₂.HCl, (CH₂O)_n, conc. HCl, ethanol, reflux, 2 h; ii) Imidazole, water, reflux, 5 h; iii) *N*-(4-Methoxyphenyl)hydrazinecarboxamide, ethanol, acetic acid, rt, 18 h

Scheme 1. Synthesis of the target semicarbazones **4**.

3.2. X-ray analysis

The asymmetric unit contains one independent molecule, as shown in Fig. 1. All the bond lengths and angles are in the normal ranges [25]. The 1,3-benzodioxole ring (C1-C6, O1, C7, and O2) forms dihedral angles of 18.62° and 22.25° with the phenyl (C15-C20) and imidazole rings (N1,C13, N2, C11 and C12), respectively. In the crystal packing, Fig. 2, molecules are linked *via* one classical intermolecular hydrogen bond and three non-classical (Table 2).

Position for Figure 1

Position for Figure 2

Table 2. Hydrogen-bond geometry (Å, °) of the title compound.

<i>D</i> — <i>H</i> ··· <i>A</i>	<i>D</i> — <i>H</i>	<i>H</i> ··· <i>A</i>	<i>D</i> ··· <i>A</i>	<i>D</i> — <i>H</i> ··· <i>A</i>
N4—H1N4···O3 ⁱ	0.90(2)	1.98(2)	2.869(2)	170(2)
C9—H9A···O3 ⁱ	0.99	2.60	3.575(3)	170
C10—H10A···O2 ⁱⁱ	0.99	2.45	3.379(3)	155
C20—H20A···O3	0.95	2.33	2.922(3)	120
C21—H21A···O1 ⁱⁱⁱ	0.98	2.48	3.217(3)	132
Symmetry codes: (i) $-x+2, -y+1, -z+1$; (ii) $-x+1, -y+1, -z+1$; (iii) $x+1, -y+3/2, z+1/2$.				

3.3. Computational studies

3.3.1. Geometry optimization

The geometrical optimisation was carried out using the B3LYP/6-311++G(d,p) basis set and the optimised molecular structure is shown in Fig. 3. The global minimum energy for optimisation of the title compound was found to be -1387.86 hartrees. The bond lengths, bond angles and dihedral angles are presented in Table 3. The optimised parameters were calculated in the gas phase and compared with the XRD results. The statistical linear regression plots between the experimental XRD values and theoretical geometrical parameters, such as bond lengths and angles, showed good agreement, as shown in Figs. S1a and b. The R^2 values for bond lengths and bond angles are 0.9913 and 0.9370, respectively. The root-mean square deviation (RMSD) value of the theoretical bond lengths from the experimental XRD values was calculated to be 0.0197 Å. Likewise, the RMSD value for the predicted bond angles was found to be 0.3663° from their experimental XRD results. This indicates that the calculated bond lengths and bond angles are in better agreement with the experimental XRD values. C15-N16 manifested the shortest C-N bond length (1.291 Å), while C41-N44 displayed the longest C-N bond length (1.4558 Å), which is shorter than the normal C-N bond length (1.480 Å). The conjugation of π -type electrons of the carbonyl group and nitrogen atom causes the possible deviation of the bond lengths of C19-N17 (1.4053 Å)

and C19-N21 (1.3621 Å). The lone pair interactions of the nitrogen atoms in the imidazole ring affect the C45-N44 (1.369 Å) and C45-N46 (1.3131 Å) bond lengths and make them shorter than other C-N bonds in the imidazole ring. The distance between O20...and H29 is 2.251 Å, which is shorter than the van der Waal's radius (2.75 Å), suggesting the possibility of hydrogen bonding (C24-H29....O20). The bond lengths between N17-H18 and N21-H22 are 1.0134 and 1.0116 Å, respectively, and they showed a slight deviation from the normal N-H bond lengths, possibly due to the carbonyl group conjugation. The calculated bond length of N16-N17 is 1.3536 Å. C38-C41 manifested a relatively longer bond length (1.5464 Å) than the other C-C bonds. The C-H bond lengths in the phenyl ring vary from 1.0795 Å (C24-H29) to 1.0857 Å (C28-H37) and it seems that the C-H bond lengths in the other rings do not deviate much. The *para* substituted phenyl ring is planar with a C19-N21-C23-C28 amide dihedral angle of 178.64°. The calculated bond angles C2-O1-C9 (105.23°), C7-O8-C9 (105.29°) and C24-C23-C28 (118.81°) seem to be consistent with the experimental values. Moreover, the computed dihedral angles of H10-C3-C4-C5 (179.86°), H12-C6-C7-C2 (178.47°) and N17-C19-N21-C23 (178.67°) closely agree with the experimental values.

Position for Figure 3

Table 3. Selected structural geometry parameters of the title compound along with the recorded XRD results.

Bond Lengths	Calculated Values (Å)	Expt. Values (Å)	Bond Angles	Calculated Values (°)	Expt. Values (°)	Dihedral Angles	Calculated Values (°)	Expt. Values (°)
O1-C2	1.3698	1.377	C2-O1-C9	105.2337	105.60	C9-O1-C2-C3	-171.920	179.36
O1-C9	1.4355	1.423	O1-C2-C3	128.9061	128.66	C9-O1-C2-C7	10.8116	-1.48
C2-C3	1.3763	1.364	O1-C2-C7	109.6409	110.27	C2-O1-C9-O8	-17.5815	2.67
C2-C7	1.3938	1.375	C3-C2-C7	121.3972	121.07	C2-O1-O9-H13	-136.289	-117.64
C3-C4	1.4041	1.396	C2-C3-C4	117.0375	117.29	C2-O1-C9-H14	100.8927	123.00
C3-H10	1.0822	0.951	C2-C3-H10	121.5067	121.37	O1-C2-C3-C4	-177.285	-179.91
C4-C5	1.4017	1.385	C4-C3-H10	121.4556	121.34	O1-C2-C3-H10	2.8252	0.03
C4-H11	1.0818	0.950	3C-4C-5C	122.23	122.00	C7-C2-C3-C4	-0.2992	1.01
C5-C6	1.4171	1.403	C3-C4-H11	117.5103	118.97	C7-C2-C3-H10	179.8108	-179.05
C5-1C15	1.4846	1.496	C5-C4-H11	120.2351	119.02	O1-C2-C7-C6	177.5332	178.98
C6-C7	1.372	1.358	C4-C5-C6	119.2841	119.17	O1-C2-C7-O8	0.233	-0.31
C6-H12	1.0807	0.949	C4-C5-C15	121.6416	121.89	C3-C2-C7-C6	0.0234	-1.79
C7-O8	1.3736	1.375	C6-C5-C15	119.0708	118.94	C3-C2-C7-O8	-177.277	178.92
O8-C9	1.433	1.423	C5-C6-C7	117.7374	117.89	C2-C3-C4-C5	-0.0265	0.21
C9-H13	1.0889	0.990	C5-C6-H12	120.7218	121.05	C2-C3-C4-H11	-178.224	-179.81
C9-H14	1.0966	0.990	C7-C6-H12	121.5337	121.07	H10-C3-C4-C5	179.8636	-179.73
C15-N16	1.291	1.278	C2-C7-C6	122.3085	122.55	H10-C3-C4-H11	1.666	0.25
C15-C38	1.5142	1.515	C2-C7-O8	109.3309	109.41	C3-C4-C5-C6	0.6158	-0.72
N16-N17	1.3536	1.371	C6-C7-O8	128.2959	128.03	C3-C4-C5-C15	-178.704	179.66
N17-H18	1.0134	0.900	C7-O8-C9	105.2907	106.18	H11-C4-C5-C6	178.7656	179.31
N17-C19	1.4053	1.382	O1-C9-O8	107.2095	108.46	H11-C4-C5-C15	-0.554	-0.32
C19-O10	1.2203	1.229	O1-C9-H13	109.422	109.95	C4-C5-C6-C7	-0.8648	0.00
C19-N21	1.3621	1.346	O1-C9-H14	109.2187	110.06	C4-C5-C6-H12	178.1835	179.94
N21-H22	1.0116	0.862	O8-C9-H13	109.5322	110.00	C15-C5-C6-C7	178.4724	179.64
N21-C23	1.4129	1.414	O8-C9-H14	109.4294	109.96	C15-C5-C6-H12	-2.4793	-0.42
C23-C24	1.3952	1.378	H13-C9-H14	111.9128	108.41	C4-C5-C15-N16	155.1131	161.61
C23-C28	1.4036	1.388	C5-C15-N16	116.5815	114.33	C4-C5-C15-C38	-28.6074	-20.82

C24-C25	1.3974	1.394	C5-C15-C38	119.9474	118.63	C6-C5-C15-N16	-24.2078	-18.02
C24-H29	1.0795	0.951	N16-C15-C38	123.359	126.99	C6-C5-C15-C38	152.0717	159.55
C25-C26	1.3945	1.377	C15-N16-N17	120.9458	122.41	C5-C6-C7-C2	0.5662	1.23
C25-H30	1.0817	0.950	N16-N17-H18	123.0733	127.45	C5-C6-C7-O8	177.3195	-179.62
C26-C27	1.3994	1.382	N16-N17-C19	122.0215	117.65	H12-C6-C7-C2	-178.474	-178.71
C26-O31	1.3678	1.379	H18-N17-C19	113.5665	114.62	H12-C6-C7-O8	-1.7206	0.44
C27-C28	1.3844	1.370	N17-C19-O20	118.9839	120.75	C2-C7-O8-C9	-11.1949	1.97
C27-H36	1.0832	0.950	N17-C19-N21	113.716	114.43	C6-C7-O8-C9	171.7128	-177.27
C28-H37	1.0857	0.950	O20-C19-N21	127.2964	124.82	C7-O8-C9-O1	17.7249	-2.87
O31-C32	1.4201	1.409	C19-N21-H22	114.53	111.72	C7-O8-C9-H13	136.3608	117.41
C32-H33	1.0958	0.980	C19-N21-C23	128.1819	128.99	C7-O8-C9-H14	-100.613	-123.27
C32-H34	1.0889	0.981	H22-N21-C23	117.2736	119.20	C5-C15-N16-N17	176.2862	179.78
C32-H35	1.0957	0.980	N21-C23-C24	123.8852	124.45	C38-C15-N16-N17	0.146	2.45
C38-H39	1.0942	0.990	N21-C23-C28	117.3035	116.65	C5-C15-C38-H39	148.9786	175.63
C38-H40	1.0893	0.990	C24-C23-C28	118.8112	118.90	C5-C15-C38-H40	31.9565	56.95
C38-C41	1.5464	1.533	C23-C24-C25	120.2076	120.30	C5-C15-C38-C41	-88.5126	-63.71
C41-H42	1.0924	0.990	C23-C24-H29	119.7105	119.81	N16-C15-C38-H39	-35.0053	-7.15
C41-H43	1.0916	0.990	C25-C24-H29	120.0818	119.89	N16-C15-C38-H40	-152.027	-125.82
C41-N44	1.4558	1.459	C24-C25-C26	120.6921	120.04	N16-C15-C38-C41	87.5035	113.52
N44-C45	1.369	1.340	C24-C25-H30	118.3096	119.90	C15-N16-N17-H18	6.9786	8.38
N44-C48	1.3823	1.358	C26-C25-H30	120.9984	120.06	C15-N16-N17-C19	172.9117	-177.98
C45-N46	1.3131	1.312	C25-C26-C27	119.0912	119.66	N16-N17-C19-O20	-176.004	-175.61
C45-H49	1.0804	0.950	C25-C26-O31	124.973	124.74	N16-N17-C19-N21	4.6533	4.37
N46-C47	1.3753	1.354	C27-C26-O31	115.9358	115.60	H18-N17-C19-O20	-8.8427	-1.16
C47-C48	1.3713	1.341	C26-C27-C28	120.2394	120.16	H18-N17-C19-N21	171.8147	178.82
C47-H50	1.0789	0.950	C26-C27-H36	118.8928	119.92	N17-C19-N21-H22	-2.7691	-1.41
C48-H51	1.0779	0.950	C28-C27-H36	120.8678	119.92	N17-C19-N21-C23	178.6681	-178.05

3.3.2. Natural bond orbital (NBO) analysis

Hyperconjugative and conjugative interactions, hydrogen bonding, intramolecular charge transfer interactions and charge delocalisation within the molecule are better explained with the help of NBO analysis. The title compound was subjected to NBO analysis using the NBO 3.1 program and the results are presented in Table 4. The charge transfer interaction from LP(1) O20 to σ^* (C24-H29) confirms the intramolecular C-H...O hydrogen bonding with an energy (E(2)) of 10.53 kcal/mol. LP(1) O20 \rightarrow σ^* C24-H29 with an energy value of 10.53 kcal/mol manifested the interaction between electron donors and acceptors. The energy of the π (C2-C3) \rightarrow π^* (C6-C7) interaction is 19.43 kcal/mol, which is greater than π (C2-C3) \rightarrow π^* (C4-C5) due to the attachment of the electronegative O8 to C7. The interaction energy of σ (C2-C3) \rightarrow σ^* (C2-C7) is 14.47 kcal/mol and it is greater than σ (C2-C3) \rightarrow σ^* (C3-C4) (12.51 kcal/mol) due to the nearby oxygen. The LP(2) O20 \rightarrow σ^* (N17-C19) interaction yielded an energy of 25.28 kcal/mol, while LP(2) O20 \rightarrow σ^* (C19-N21) gave an energy of 23.08 kcal/mol. The former energy is higher due to the attachment of N16 to N17. The interaction energies of LP(2) O31 \rightarrow σ^* (C32-H33) and LP(2) O31 \rightarrow π^* (C25-C26) are 10.71 and 28.52 kcal/mol, respectively. The higher E(2) value of the latter interaction implies that the presence of oxygen and nitrogen nearby the phenyl ring affects the intramolecular charge transfer. The lone pair LP(2) O31 interacts with the antibonding

orbital σ^* C32-H33 with an energy value of 10.71 kcal/mol, confirming the C-H...O hydrogen bonding and giving rise to the possibility of binding of the title compound to its target protein. Moreover, the results of the NBO analysis can identify the efficiency of donor and acceptor groups within the title compound, which supports its interaction with the target protein.

Table 4. Selected donor-acceptor interactions results of the title compound based on second-order perturbation theory in Fock matrix.

Donor (i)	ED (i)e	Acceptor (i)	ED (j)e	E(2) ^a (kcal/mol)	E(j)-E(i) ^b (a.u.)	F(i,j) ^c (a.u.)
π C2 - C3	1.68826	π^* C4-C5	0.38017	19.02	0.30	0.069
π C2 - C3	1.68826	π^* C6-C7	0.34163	19.43	0.30	0.069
π C4 - C5	1.68925	π^* C2-C3	0.36664	17.75	0.28	0.064
π C4 - C5	1.68925	π^* C6-C7	0.34163	17.02	0.28	0.062
π C4 - C5	1.68925	π^* C15-N16	0.23453	15.63	0.27	0.059
π C6 - C7	1.70539	π^* C2-C3	0.36664	19.90	0.29	0.070
π C6 - C7	1.70539	π^* C4-C5	0.38017	18.03	0.30	0.067
σ C2 - C3	1.97482	σ^* C2-C7	0.03933	14.47	1.27	0.068
σ C2 - C3	1.97482	σ^* C3-C4	0.01177	12.51	1.29	0.051
π C23 - C24	1.66396	π^* C25-C26	0.39083	18.36	0.28	0.065
π C25 - C26	1.67132	π^* C23-C24	0.38080	20.47	0.29	0.070
π C27 - C28	1.73229	π^* C23-C24	0.38080	17.94	0.29	0.066
π C27 - C28	1.73229	π^* C25-C26	0.39083	18.93	0.29	0.068
π C47 - C48	1.85707	π^* C45-N46	0.37848	15.10	0.28	0.061
LP (2) O1	1.85282	π^* C2-C3	0.36664	26.94	0.35	0.092
LP (2) O8	1.85920	π^* C6-C7	0.34163	26.03	0.36	0.091
LP (1) N16	1.91031	σ^* C15-C38	0.03546	10.80	0.78	0.083
LP (1) N17	1.70419	π^* C15-N16	0.23453	31.90	0.29	0.087
LP (2) O20	1.84694	σ^* N17-C19	0.08098	25.28	0.64	0.116
LP (2) O20	1.84694	σ^* C19-N21	0.07040	23.08	0.71	0.117
LP (1) O20	1.97871	σ^* C24-H29	0.01421	10.53	1.17	0.022
LP (1) N21	1.68358	π^* C23-C24	0.38080	32.67	0.30	0.090
LP (2) O31	1.84921	π^* C25-C26	0.39083	28.52	0.34	0.094
LP (2) O31	1.84921	σ^* C32-H33	0.01950	10.71	0.69	0.058
LP (1) N44	1.56078	π^* C45-N46	0.37848	45.67	0.28	0.102

^aEnergy of hyperconjugative interactions; ^bEnergy difference between donor and acceptor i and j NBO orbitals; ^cFock matrix element between i and j NBO orbitals.

3.3.3. Natural population analysis (NPA) and Molecular electrostatic potential (MEP)

The calculation of atomic charges plays an important role in molecular systems. Molecular properties, like electronic structure, molecular polarisability and dipole moment, are influenced by atomic charges. The atomic charges of the title compound were calculated by natural population analysis. It is an effective method to calculate the atomic charges within the molecule and it gives the exact charge on the atoms. Natural population analysis of the title compound was calculated using the DFT/B3LYP/6-311++G(d,p) level of basis set. A plot of the charge distribution is shown in Fig. 4. Carbon atom C19 (0.8038 e) manifested the

highest positive charge in the title molecule due to its direct attachment with the electronegative atoms O20, N17 and N21 and O20 participates in the C24-H29...O20 hydrogen bonding. Moreover, the carbon atoms C2 (0.274 e), C7 (0.267 e), C9 (0.305 e), C15 (0.225 e), C23 (0.132 e), C26 (0.302 e) and C45 (0.206 e) showed more positive charges than the other carbon atoms in the molecule due to their direct attachment to either oxygen or nitrogen electronegative atoms. All hydrogen atoms showed positive charges, whereas H18 and H22 displayed more positive charges owing to their direct attachment to N17 and N21, respectively.

Position for Figure 4

The molecular electrostatic potential (MEP) analysis helps the understanding of relative polarity, partial charges and sites of chemical reactivity and hydrogen bonding of the molecule. The molecular electrostatic potential maps of the title compound in solid, mesh and transparent forms are shown in Fig. S2 a, b and c, respectively. The MEP map of the title molecule is in the range of $-5.638e \times 10^{-2}$ to $5.638e \times 10^{-2}$. Its range of electrostatic potential can be analysed by different colour codes. Electrostatic potential is in the following order: red < orange < yellow < green < blue. In the MEP plot the regions around the electronegative atoms like oxygen and nitrogen have negative potential and shows slight red and orange colours. Whereas, the carbon and hydrogen atoms have positive potential and the regions around these atoms show green and blue colours. The red colour around O20 atom suggests the possibility of formation of C24-H29...O20 hydrogen bonding.

3.3.4. Frontier molecular orbital (FMO) analysis

The kinetic stability of a molecule is determined by the highest occupied molecular orbital (HOMO) and lowest unoccupied molecular orbital (LUMO), and their energy gap reflects the chemical reactivity of the molecule. The frontier molecular orbital plays an important role in the electric and optical properties of the molecule [26]. The HOMO, LUMO and their energy gap for the title compound were calculated using the DFT/B3LYP/6-311++G(d,p) level of basis set. The HOMO value is related to the ionisation potential ($IP = -E_{HOMO}$), whereas the LUMO value is related to the electron affinity ($EA = -E_{LUMO}$). HOMO and LUMO plots are shown in Fig. 5. The HOMO is mainly localised on the phenyl ring, while the LUMO is localised on the benzodioxole ring. The HOMO and LUMO energies were found to be -5.72 and -1.81 eV, respectively, and the calculated value of the energy gap is 3.91 eV. The HOMO-LUMO energy gap reveals the possibility of intramolecular charge

transfer within the molecule. The global hardness (η) and softness (σ) of the title molecule are 1.96 eV and 0.51 (eV)^{-1} using the relations $\eta = \text{IP} - \text{EA} / 2$ and $\sigma = 1 / \eta$, respectively.

Position for Figure 5

3.3.5. Vibrational spectral analysis

The spectroscopic properties of the title compound are analysed by FT-IR, FT-Raman and the vibrational frequencies are calculated using DFT and compared with the experimental data. The observed and simulated FT-IR and FT-Raman spectra are shown in Figs. 6 and 7, respectively. The computed and experimental wavenumbers and their assignments with potential energy distribution (PED) values are presented in Table 5.

- Position for Figure 6
- Position for Figure 7

Table 5. Vibrational assignments of the title compound based on potential energy distribution analysis.

Calculated wavenumbers (cm^{-1})	Experimental wavenumbers (cm^{-1})		Assignment with PED (%)
	IR	Raman	
3462	3451 vw	-	ν N21-H22 (99) Amide
3399	3381 s	-	ν N17-H18
3325	3316 w	-	ν N21-H22
3203	3197 s	-	ν N17-H18
3132	3132 m	-	ν C48-H51 (24), C47-H50 (75)
3090	3078 m	3079 m	ν C27-H36 (95)
2998	3001 m		ν 41C-43H (92)
2960	2963 m	2964 m	ν_{as} CH ₂ (92) MeI (42)
2944	2936 m		ν_{as} CH ₂ (91) MeII (88)
2903	2894 m	2902 w	ν C38-H39 (88)
1664	1660 vs	1667 w	ν C19=O20 (77)
1604	1609 s	1618 s	ν C27-C28 (33)
1580	-	1580 vs	ν N16-C15 (33)
1519	1519 vs	1509 m	ν C19-N21 (14)
1441	1436 vs	1438 s	δ H42-C41-H43 (53)
1398	-	1395 w	β H29-C24-C25 (10)
1346	-	1351 w	W H42-C41-H43 (48)
1339	1338 s		β H50-C47-C48 (10)
1311	1304 s		β C23-C28 (10), C23-C24 (17), C25-C26 (12)
1288		1287 w	δ H29-C24-C25 (12), H30-C25-C26 (10)
1267	1277 s		β H50-C47-C48 (25), H51-C48-C47 (13)
1240	1242 vs		δ H40-C38-C15-C5 (17)
1175	1179 s	1179 w	ν_{R} H13-C9-O8 (74)
1129	1135 s	1134 w	ρ -OCH ₃ (83)
1103	1102 s	-	β C9-O1-O8-H13 (76), H37-C28-C27 (16), H36-C27-C28 (25)
1032	1038 vs	1044 w	W H39-C38-H40 (39)
994	997 m	-	γ C23-C28 (20), C24-C25-C26 (10)
933	947 m	-	γ C24-C23-C25-H29 (56), H30-C25-C26-O31 (20), H36-C27-C28-H37 (12)
916	920 w	-	γ C7-C2-O1 (67)

882		875 w	Y C3-C4-C5 (22)
853	858 w	-	vC19-N21 (15),N21-C23 (13),C23-C24 (17)
838	827 m	-	Y H51-C48-C47-N46 (11),C47-C48-N46-H50 (81)
804		807 w	Y O1-C2-C3 (14)
800	800 m	-	Y C2-C7-C6 (20)
749	750 m	-	ρ H39-C38-C15-C5 (11), H42-C41-N44-C45 (19)
668	664 m	-	δ N17-C19=O20 (14)
615	619 w	-	Y N44-C48-C47-N46 (54)
585	591 m	-	τ C25-C26-C27 (12),C5-C15-N16 (10)
509	512 w	-	τ C24-C25-C26-C27 (55),C28-C27-C26-O31 (20)
454	464 vw	-	δ C3-C2-C7 (16),N17-C19-O20 (12)

v – stretching, v_{as} -asymmetric stretching, v_R –ring stretching, β – in plane bending, W – wagging, d – deformation, ρ – rocking, δ – bending, Y – out of plane bending, τ – torsion, Me I- methylene I, Me II - methylene II, , vs- very strong, s- strong, m- medium, w- weak, vw- very weak.

3.3.5.1. Imidazol ring vibrations

The calculated FT-IR imidazole C-H stretching vibrations appeared at 3145–3115 cm^{-1} and were observed at 3132 cm^{-1} . Imidazole ring C=C stretching vibrations normally appear in the region of 1605–1585 cm^{-1} [27] and this vibration is experimentally recorded as a strong absorption band at 1580 cm^{-1} in the FT-Raman spectrum of the title compound. The C-H in-plane bending vibrations were observed at 1395 cm^{-1} in the FT-Raman spectrum of the title compound and at 1338, 1304 and 1277 cm^{-1} with strong intensities in its FT-IR spectrum, which agrees with the literature data. The C-H out-of-plane bending and torsional vibrations are observed at 619, 591 and 512 cm^{-1} in the FT-IR spectrum of the title compound.

3.3.5.2. Benzodioxole ring vibrations

C-H stretching vibrations are normally observed in the region of 3100–3000 cm^{-1} [28]. A FT-IR band of medium intensity at 3001 cm^{-1} was assigned to this vibration in the title compound. The ring stretching C-C vibration was observed at 1179 cm^{-1} for both FT-IR and FT-Raman spectra of the title compound. The strong FT-IR absorption band at 1102 cm^{-1} corresponds to the C-H in-plane bending mode. The C-H out-of-plane bending vibrations are also observed for the title compound at 920, 827 and 800 cm^{-1} in the FT-IR spectrum and at 875 and 807 cm^{-1} in the FT-Raman spectrum, in agreement with the reported values.

3.3.5.3. Methylene groups vibrations

Asymmetric stretching vibrations of methylene groups are reported in the region of 2930 cm^{-1} [28]. The methylene groups in the title compound showed an asymmetric stretching band of medium intensity at 2936 cm^{-1} in its FT-IR spectrum. The CH₂ vibrations are reported in the region of 2926–2855 cm^{-1} [29] and were observed at 2902 and 2894 cm^{-1} in the FT-Raman and FT-IR spectra of the title compound, respectively. The twisting and wagging vibrations usually appear at 1422–719 cm^{-1} and they were noticed at 1351 cm^{-1} in the FT-Raman spectrum of the title compound and at 750 cm^{-1} in its FT-IR spectrum.

3.3.5.4. Carboxamide (secondary amide) vibrations

The absorption bands of amides are influenced by the hydrogen bonding and the substituents on the nitrogen atom. Amide N-H stretching vibrations usually occur in the region of 3460–3300 cm^{-1} [30], which was noticed as weak to strong absorptions at 3451, 3316, 3381 and 3197 cm^{-1} in the FT-IR spectrum of the title molecule. The C=O stretching vibrations normally show peaks at 1680–1630 cm^{-1} . The title compound manifested a very strong C=O peak at 1660 cm^{-1} in its FT-IR spectrum and as a weak band at 1667 cm^{-1} in its FT-Raman spectrum. Due to N-H bending motion, secondary amides have absorption bands in the range of 1570–1515 cm^{-1} and they were observed as a very strong FT-IR band at 1519 cm^{-1} and as a medium band at 1509 cm^{-1} in the FT-Raman spectrum of the title molecule. The bending motion of the O=C-N group causes amides to have bands in the region of 695–550 cm^{-1} , which was observed as a medium band at 664 cm^{-1} in the FT-IR spectrum of the title molecule. Amides also show absorption bands in the region of 520–430 cm^{-1} , which occurred at 464 cm^{-1} in the FT-IR spectrum of the title compound.

3.3.5.5. Phenyl ring vibrations

The aromatic C-H stretching vibrations of the phenyl ring usually appear at 3080–3010 cm^{-1} [28], which were noted as medium intense bands at 3079 and 3078 cm^{-1} in the FT-Raman and FT-IR spectra of the title compound, respectively. Strong bands at 1618 and 1609 cm^{-1} in the FT-Raman and FT-IR spectra of the title compound, respectively, correspond to the aromatic C=C stretching vibrations, which normally appear in the region of 1625–1430 cm^{-1} [30]. The in-plane C-H deformation vibrations occur at 1290–1000 cm^{-1} and the band observed at 1287 cm^{-1} in FT-Raman spectrum of the title compound and a very strong absorption at 1242 cm^{-1} in its FT-IR were assigned to this vibration. The C-H out-of-plane vibrations were noticed at 997 and 947 cm^{-1} in the FT-IR spectrum of the title molecule, which usually fall in the region of 1000–700 cm^{-1} .

3.3.5.6. Methoxy group vibrations

Asymmetric methoxy vibrations normally lie between 3030 and 2950 cm^{-1} [29]. The medium intense bands at 2964 cm^{-1} in the FT-Raman spectrum of the title molecule and at 2963 cm^{-1} in its FT-IR spectrum were assigned to these vibrations. Asymmetric methoxy deformation occurs in the region of 1475–1435 cm^{-1} and it was noticed at 1438 and 1436 cm^{-1} in the FT-Raman and FT-IR spectra of the title compound, respectively, with strong absorption. The OCH₃ rocking vibrations were reported at 1190–1100 cm^{-1} and were manifested at 1134 cm^{-1} in the FT-Raman spectrum of the title compound and at 1135 cm^{-1} in its FT-IR spectrum.

3.3.5.7. Skeletal mode vibrations

The C-N and C-C stretching vibrations usually appear in the 1150–850 cm^{-1} region [30]. The C-N vibrations are difficult to identify as they usually couple with other bands. A weak band was observed at 858 cm^{-1} in the FT-IR spectrum of the title molecule, which is attributed to this vibration.

3.4. Antifungal activity

The antifungal activity of the title compound was assessed *in vitro* against *C. albicans*, *C. tropicalis*, *C. parapsilosis* as well as *A. niger* fungal strains according to the literature procedure [15] and the results are illustrated in Table 6. The title molecule exhibited a MIC value of 0.628 $\mu\text{mol/mL}$ against *C. albicans*, *C. parapsilosis* and *A. niger*, while it showed a MIC value of 0.314 $\mu\text{mol/mL}$ against *C. tropicalis*.

Table 6. Antifungal activity of the title compound towards *C. albicans*, *C. tropicalis*, *C. parapsilosis* and *A. niger*.

Compound No.	MIC ($\mu\text{mol/mL}$)			
	<i>Candida albicans</i>	<i>Candida tropicalis</i>	<i>Candida parapsilosis</i>	<i>Asperagillus niger</i>
4	0.628	0.314	0.628	0.628
Fluconazole	0.051	0.045	0.047	ND
Ketoconazole	ND	ND	ND	0.02

3.5. Molecular docking studies

Molecular docking is used to predict the binding orientation of small drug candidate molecules to their protein targets. Hence, docking plays an important role in rational drug design. AutoDock is an automated procedure for predicting the interaction of ligands with bio macromolecular targets. In the present study, AutoDock 4.2 software interfaced with AutoDockTools v1.5.6rc3 based on the Lamarckian genetic algorithm [24] was used to perform molecular docking investigations. The X-ray crystal structure of human CYP3A4 (PDB Code :4D6Z) [31] with a resolution of 1.93 Å was selected from the Research Collaboratory for Structural Bioinformatics protein data bank. CYP3A4 is involved in the metabolism of xenobiotics and can enhance the therapeutic efficiency of the co-administered pharmaceuticals that are metabolized by CYP3A4.

Rigid docking was performed by the AutoDockTools program and visualised using PyMOL v1.2r1 [32]. The grid box size of 100 × 100 × 100 points was set with a spacing of 0.79 Å over the target protein binding pocket.

The predicted of C-H...O hydrogen bonding NBO analysis, stabilises the protein-ligand interaction. The amino acid residue ARG 105 in the active site of the CYP3A4 protein interacts with the title molecule by C-H...O hydrogen bonding and stabilises the CYP3A4-ligand complex (Fig. 8). While, the presence of phenyl group in the title molecule increases its binding affinity.

Out of 100 genetic algorithm runs, the best docked conformation had a binding energy of -8.88 kcal/mol with an estimated inhibition constant of 310.7 nM. The binding affinity of the title compound to the CYP3A4 protein might be beneficial and promote the biological activity of the simultaneous administered bioactive compounds that are metabolised by CYP3A4.

Position for Figure 8

4. Conclusions

The molecular hybrid (*E*)-2-(1,3-benzodioxol-5-yl)-3-(1*H*-imidazol-1-yl)propylidene-*N*-(4-methoxyphenyl)hydrazinecarboxamide was synthesised to be evaluated as a new antifungal candidate. The assigned chemical structure of the title compound was confirmed using different spectroscopic techniques. The (*E*)-configuration of the imine double bond of the title compound was unambiguously determined *via* its single crystal X-ray analysis. DFT computations were carried out at the DFT/B3LYP method. The optimised geometric parameters and the calculated vibrational frequencies are in a good agreement with the experimental values. Charge transfer interactions within the title molecule were explored by HOMO-LUMO investigations and NBO analysis suggested possible hydrogen bonding formation. *In vitro* antifungal screening of the title compound towards four fungal strains revealed its antifungal activity against *C. tropicalis* with a MIC value of 0.314 $\mu\text{mol/mL}$ and against *C. albicans*, *C. parapsilosis* and *A. niger* with a MIC value of 0.628 $\mu\text{mol/mL}$. Moreover, the molecular docking study showed the possible binding mode of the title compound to the 4D6Z protein. It is believed that the results of the current study could be harnessed to support the development of new potent and safe antifungal drug-like candidates.

Acknowledgments: The authors would like to extend their sincere appreciation to the Deanship of Scientific Research at King Saud University for its funding of this research through the Research Group Project No. RG-1438-083.

References

- [1] A.H. Groll, J. Lumb, New developments in invasive fungal disease, *Future Microbiol.* 7 (2) (2012) 179–184.

- [2] P. Vandeputte, S. Ferrari, A.T. Coste, Antifungal resistance and new strategies to control fungal infections, *Int. J. Microbiol.* 2012 (2011) 1–24, Article ID 713687.
- [3] S. Crunkhorn, Fungal infection: Protecting from *Candida albicans*, *Nat. Rev. Drug Discov.* 15 (9) (2016) 604–604.
- [4] M.C. Arendrup, Epidemiology of invasive candidiasis, *Curr. Opin.Crit. Care* 16 (5) (2010) 445–452.
- [5] S.K.J. Shaikh, R.R. Kamble, S.M. Somagond, H. Devarajegowda, S.R. Dixit, S.D. Joshi, Tetrazolylmethyl quinolines: Design, docking studies, synthesis, anticancer and antifungal analyses, *Eur. J. Med. Chem.* 128 (2017) 258–273.
- [6] J. Heeres, L. Meerpoel, P. Lewi, Conazoles, *Molecules* 15 (6) (2010) 4129–4188.
- [7] C. Onyewu, J.R. Blankenship, M. Del Poeta, J. Heitman, Ergosterol biosynthesis inhibitors become fungicidal when combined with calcineurin inhibitors against *Candida albicans*, *Candida glabrata*, and *Candida krusei*, *Antimicrob. Agents Chemother.* 47 (3) (2003) 956–964.
- [8] H. Hof, A new, broad-spectrum azole antifungal: posaconazole—mechanisms of action and resistance, spectrum of activity, *Mycoses* 49 (s1) (2006) 2–6.
- [9] L. Jafri, F.L. Ansari, M. Jamil, S. Kalsoom, S. Qureishi, B. Mirza, Microwave-assisted synthesis and bioevaluation of some semicarbazones, *Chem. Biol. Drug Des.* 79 (6) (2012) 950–959.
- [10] M.J. Ahsan, M. Amir, M.A. Bakht, J.G. Samy, M.Z. Hasan, M.S. Nomani, Synthesis and antimicrobial activity of *N*-1-(3-chloro-4-fluorophenyl)-*N*-4-substituted semicarbazone derivatives, *Arab. J. Chem.* 9 (2016) S861–S866.
- [11] N. Micale, M. Zappalà, S. Grasso, Synthesis and cytotoxic activity of 1,3-benzodioxole derivatives. Note II, *Il Farmaco*, 58 (5) (2003) 351–355.
- [12] A.C.L. Leite, K.P. da Silva, I.A. de Souza, J.M. de Araújo, D.J. Brondani, Synthesis, antitumour and antimicrobial activities of new peptidyl derivatives containing the 1, 3-benzodioxole system, *Eur. J. Med. Chem.* 39 (12) (2004) 1059–1065.
- [13] M.N. Aboul-Enein, A.A. El-Azzouny, M.I. Attia, Y.A. Maklad, K.M. Amin, M. Abdel-Rehim, M.F. El-Behairy, Design and synthesis of novel stiripentol analogues as potential anticonvulsants, *Eur. J. Med. Chem.* 47 (2012) 360–369.
- [14] A. Hall, S.H. Brown, A. Chowdhury, G.M. Giblin, M. Gibson, M.P. Healy, D.G. Livermore, R.J.M. Wilson, A. Naylor, D.A. Rawlings, Identification and

- optimization of novel 1, 3, 4-oxadiazole EP 1 receptor antagonists, *Bioorg. Med. Chem. Lett.* 17 (16) (2007) 4450–4455.
- [15] R.I. Al-Wabli, A.R. Al-Ghamdi, H.A. Ghabbour, M.H. Al-Agamy, J.C. Monicka, I.H. Joe, M.I. Attia, Synthesis, x-ray single crystal structure, molecular docking and DFT computations on *N*-[(1*E*)-1-(2*H*-1,3-benzodioxol-5-yl)-3-(1*H*-imidazol-1-yl)propyl idene]hydroxylamine: A new potential antifungal agent precursor, *Molecules*, 22 (3) (2017) 373.
- [16] G. Scheldrick, A short history of SHELX, *Acta Crystallogr A* 64 (2008) 112–122.
- [17] G. Sheldrick, SHELXL\PC V6. 1 Windows NT Version, Bruker analytical x-ray systems Inc.: Madison, WI, (2001).
- [18] M. Frisch, G. Trucks, H. Schlegel, G. Scuseria, M. Robb, J. Cheeseman, G. Scalmani, V. Barone, B. Mennucci, G. Petersson, 09, Revision A. 02, Gaussian Inc, Wallingford, CT, (2009).
- [19] C. Lee, W. Yang, R.G. Parr, Development of the Colle-Salvetti correlation-energy formula into a functional of the electron density, *Phys. Rev. B* 37 (2) (1988) 785.
- [20] A.D. Becke, Density-functional thermochemistry. IV. A new dynamical correlation functional and implications for exact-exchange mixing, *J. Chem. Phys.*, 104 (3) (1996) 1040–1046.
- [21] A.P. Scott, L. Radom, Harmonic vibrational frequencies: an evaluation of Hartree– Fock, Møller– Plesset, quadratic configuration interaction, density functional theory, and semiempirical scale factors, *J. Phys. Chem.* 100 (41) (1996) 16502–16513.
- [22] M.H. Jamróz, Vibrational energy distribution analysis (VEDA): scopes and limitations, *Spectrochim. Acta A: Mol. Biomol. Spectrosc.* 114 (2013) 220–230.
- [23] E. Glendening, A. Reed, J. Carpenter, F. Weinhold, NBO, Theoretical Chemistry Institute, University of Wisconsin, Madison, USA, (2001).
- [24] G.M. Morris, R. Huey, W. Lindstrom, M.F. Sanner, R.K. Belew, D.S. Goodsell, A.J. Olson, AutoDock4 and AutoDockTools4: Automated docking with selective receptor flexibility, *J. Comput. Chem.* 30 (16) (2009) 2785–2791.

- [25] F.H. Allen, O. Kennard, D.G. Watson, L. Brammer, A.G. Orpen, R. Taylor, Tables of bond lengths determined by X-ray and neutron diffraction. Part 1. Bond lengths in organic compounds, *J. Chem. Soc. Perkin Trans. II* 12 (1987) S1–S19.
- [26] M. Sreenath, S. Mathew, I.H. Joe, V. Rastogi, Z-scan measurements of the third-order optical nonlinearities and vibrational spectral studies by DFT computations on azo dye 1-(2-methylphenylazo)-2-naphthol, *Opt. Laser Technol.* 97 (2017) 390–399.
- [27] Y. Ünver, K. Sancak, H. Tanak, İ. Değirmencioğlu, E. Düğdü, M. Er, Ş. Işık, 5-benzyl-4-[3-(1*H*-imidazol-1-yl)propyl]-2*H*-1,2,4-triazol-3(4*H*)-ones: Synthesis, spectroscopic characterization, crystal structure and a comparison of theoretical and experimental IR results by DFT calculations, *J. Mol. Struct.* 936 (1) (2009) 46–55.
- [28] M. Tammer, G. Sokrates: Infrared and Raman characteristic group frequencies: tables and charts, *Colloid Polym. Sci.* 283 (2) (2004) 235–235.
- [29] N. Colthup, *Introduction to infrared and Raman spectroscopy*, Elsevier, 2012.
- [30] B.C. Smith, *Infrared spectral interpretation: a systematic approach*, CRC press, 1998.
- [31] P. Kaur, A.R. Chamberlin, T.L. Poulos, I.F. Sevrioukova, Structure-based inhibitor design for evaluation of a CYP3A4 pharmacophore model, *J. Med. Chem.* 59 (9) (2015) 4210–4220.
- [32] W. DeLano, *The PyMOL Molecular Graphics System*. San Carlos, CA: DeLano Scientific; 2002, in, Accessed 6/25/2007. Available at <http://www.pymol.org>, 2010.

Figures captions

Scheme 1. Synthesis of the target semicarbazone **4**.

Fig. 1. ORTEP diagram of the titled compound. Displacement ellipsoids are plotted at the 40% probability level for non-hydrogen atoms.

Fig. 2. Molecular packing of titled compound viewed hydrogen bonds which are drawn as dashed lines along *a* axis.

Fig. 3. Optimized molecular structure of the title compound.

Fig. 4. Charge distribution chart for the title compound according to the natural population analysis.

Fig. 5. HOMO (upper) and LUMO (lower) energy plots of the title compound.

Fig. 6. (a) Experimental (b) Simulated infrared spectra of the title compound in the region 4000-500 cm^{-1} .

Fig. 7. (a) Experimental (b) Simulated Raman spectra of the title compound in the region 3500-50 cm^{-1} .

Fig. 8. Binding pose diagram with protein-ligand interactions of the title compound.

Table 1. Experimental X-ray details the title compound.

Crystal data	
Chemical formula	C ₂₁ H ₂₁ N ₅ O ₄
Mr	407.43
Crystal system, space group	Monoclinic, <i>P</i> 2 ₁ / <i>c</i>
Temperature (K)	296
<i>a</i> , <i>b</i> , <i>c</i> (Å)	10.7007 (4), 7.3072 (3), 24.9088 (8)
β (°)	97.178 (2)
<i>V</i> (Å ³)	1932.41 (12)
<i>Z</i>	4
Radiation type	Cu <i>K</i> α
μ (mm ⁻¹)	0.82
Crystal size (mm)	0.36 × 0.15 × 0.11
Data collection	
Diffractometer	Bruker APEX-II D8 venture diffractometer
Absorption correction	Multi-scan SADABS Bruker 2014
Tmin, Tmax	0.757, 0.913
No. of measured, independent and observed [<i>I</i> > 2 σ (<i>I</i>)] reflections	9324, 3380, 2388
<i>R</i> _{int}	0.039
Refinement	
<i>R</i> [<i>F</i> ² > 2 σ (<i>F</i> ²)], <i>wR</i> (<i>F</i> ²), <i>S</i>	0.049, 0.132, 1.06
No. of reflections	3380
No. of parameters	280
No. of restraints	0
H-atom treatment	H atoms treated by a mixture of independent and constrained refinement
$\Delta\rho_{\max}$, $\Delta\rho_{\min}$ (e Å ⁻³)	0.22, -0.23

Table 2. Hydrogen-bond geometry (Å, °) the title compound.

<i>D</i> — <i>H</i> ··· <i>A</i>	<i>D</i> — <i>H</i>	<i>H</i> ··· <i>A</i>	<i>D</i> ··· <i>A</i>	<i>D</i> — <i>H</i> ··· <i>A</i>
N4—H1N4···O3 ⁱ	0.90(2)	1.98(2)	2.869(2)	170(2)
C9—H9A···O3 ⁱ	0.99	2.60	3.575(3)	170
C10— H10A···O2 ⁱⁱ	0.99	2.45	3.379(3)	155
C20—H20A···O3	0.95	2.33	2.922(3)	120
C21— H21A···O1 ⁱⁱⁱ	0.98	2.48	3.217(3)	132
Symmetry codes: (i) $-x+2, -y+1, -z+1$; (ii) $-x+1, -y+1, -z+1$; (iii) $x+1, -y+3/2, z+1/2$.				

Table 3. Selected structural geometry parameters of the title compound along with the recorded XRD results.

Bond Length	Calculated Value (Å)	Expt. Value (Å)	Bond Angle	Calculated Value ($^{\circ}$)	Expt. Value ($^{\circ}$)	Dihedral Angle	Calculated Value ($^{\circ}$)	Expt. Value ($^{\circ}$)
O1-C2	1.3698	1.377	C2-O1-C9	105.2337	105.60	C9-O1-C2-C3	-171.920	179.36
O1-C9	1.4355	1.423	O1-C2-C3	128.9061	128.66	C9-O1-C2-C7	10.8116	-1.48
C2-C3	1.3763	1.364	O1-C2-C7	109.6409	110.27	C2-O1-C9-O8	-17.5815	2.67
C2-C7	1.3938	1.375	C3-C2-C7	121.3972	121.07	C2-O1-O9-H13	-136.289	-117.64
C3-C4	1.4041	1.396	C2-C3-C4	117.0375	117.29	C2-O1-C9-H14	100.8927	123.00
C3-H10	1.0822	0.951	C2-C3-H10	121.5067	121.37	O1-C2-C3-C4	-177.285	-179.91
C4-C5	1.4017	1.385	C4-C3-H10	121.4556	121.34	O1-C2-C3-H10	2.8252	0.03
C4-H11	1.0818	0.950	3C-4C-5C	122.23	122.00	C7-C2-C3-C4	-0.2992	1.01
C5-C6	1.4171	1.403	C3-C4-H11	117.5103	118.97	C7-C2-C3-H10	179.8108	-179.05
C5-IC15	1.4846	1.496	C5-C4-H11	120.2351	119.02	O1-C2-C7-C6	177.5332	178.98
C6-C7	1.372	1.358	C4-C5-C6	119.2841	119.17	O1-C2-C7-O8	0.233	-0.31
C6-H12	1.0807	0.949	C4-C5-C15	121.6416	121.89	C3-C2-C7-C6	0.0234	-1.79
C7-O8	1.3736	1.375	C6-C5-C15	119.0708	118.94	C3-C2-C7-O8	-177.277	178.92
O8-C9	1.433	1.423	C5-C6-C7	117.7374	117.89	C2-C3-C4-C5	-0.0265	0.21
C9-H13	1.0889	0.990	C5-C6-H12	120.7218	121.05	C2-C3-C4-H11	-178.224	-179.81
C9-H14	1.0966	0.990	C7-C6-H12	121.5337	121.07	H10-C3-C4-C5	179.8636	-179.73
C15-N16	1.291	1.278	C2-C7-C6	122.3085	122.55	H10-C3-C4-H11	1.666	0.25
C15-C38	1.5142	1.515	C2-C7-O8	109.3309	109.41	C3-C4-C5-C6	0.6158	-0.72
N16-N17	1.3536	1.371	C6-C7-O8	128.2959	128.03	C3-C4-C5-C15	-178.704	179.66
N17-H18	1.0134	0.900	C7-O8-C9	105.2907	106.18	H11-C4-C5-C6	178.7656	179.31
N17-C19	1.4053	1.382	O1-C9-O8	107.2095	108.46	H11-C4-C5-C15	-0.554	-0.32
C19-O10	1.2203	1.229	O1-C9-H13	109.422	109.95	C4-C5-C6-C7	-0.8648	0.00
C19-N21	1.3621	1.346	O1-C9-H14	109.2187	110.06	C4-C5-C6-H12	178.1835	179.94
N21-H22	1.0116	0.862	O8-C9-H13	109.5322	110.00	C15-C5-C6-C7	178.4724	179.64
N21-C23	1.4129	1.414	O8-C9-H14	109.4294	109.96	C15-C5-C6-H12	-2.4793	-0.42
C23-C24	1.3952	1.378	H13-C9-H14	111.9128	108.41	C4-C5-C15-N16	155.1131	161.61
C23-C28	1.4036	1.388	C5-C15-N16	116.5815	114.33	C4-C5-C15-C38	-28.6074	-20.82
C24-C25	1.3974	1.394	C5-C15-C38	119.9474	118.63	C6-C5-C15-N16	-24.2078	-18.02
C24-H29	1.0795	0.951	N16-C15-C38	123.359	126.99	C6-C5-C15-C38	152.0717	159.55
C25-C26	1.3945	1.377	C15-N16-N17	120.9458	122.41	C5-C6-C7-C2	0.5662	1.23

C25-H30	1.0817	0.950	N16-N17-H18	123.0733	127.45	C5-C6-C7-O8	177.3195	-179.62
C26-C27	1.3994	1.382	N16-N17-C19	122.0215	117.65	H12-C6-C7-C2	-178.474	-178.71
C26-O31	1.3678	1.379	H18-N17-C19	113.5665	114.62	H12-C6-C7-O8	-1.7206	0.44
C27-C28	1.3844	1.370	N17-C19-O20	118.9839	120.75	C2-C7-O8-C9	-11.1949	1.97
C27-H36	1.0832	0.950	N17-C19-N21	113.716	114.43	C6-C7-O8-C9	171.7128	-177.27
C28-H37	1.0857	0.950	O20-C19-N21	127.2964	124.82	C7-O8-C9-O1	17.7249	-2.87
O31-C32	1.4201	1.409	C19-N21-H22	114.53	111.72	C7-O8-C9-H13	136.3608	117.41
C32-H33	1.0958	0.980	C19-N21-C23	128.1819	128.99	C7-O8-C9-H14	-100.613	-123.27
C32-H34	1.0889	0.981	H22-N21-C23	117.2736	119.20	C5-C15-N16-N17	176.2862	179.78
C32-H35	1.0957	0.980	N21-C23-C24	123.8852	124.45	C38-C15-N16-N17	0.146	2.45
C38-H39	1.0942	0.990	N21-C23-C28	117.3035	116.65	C5-C15-C38-H39	148.9786	175.63
C38-H40	1.0893	0.990	C24-C23-C28	118.8112	118.90	C5-C15-C38-H40	31.9565	56.95
C38-C41	1.5464	1.533	C23-C24-C25	120.2076	120.30	C5-C15-C38-C41	-88.5126	-63.71
C41-H42	1.0924	0.990	C23-C24-H29	119.7105	119.81	N16-C15-C38-H39	-35.0053	-7.15
C41-H43	1.0916	0.990	C25-C24-H29	120.0818	119.89	N16-C15-C38-H40	-152.027	-125.82
C41-N44	1.4558	1.459	C24-C25-C26	120.6921	120.04	N16-C15-C38-C41	87.5035	113.52
N44-C45	1.369	1.340	C24-C25-H30	118.3096	119.90	C15-N16-N17-H18	6.9786	8.38
N44-C48	1.3823	1.358	C26-C25-H30	120.9984	120.06	C15-N16-N17-C19	172.9117	-177.98
C45-N46	1.3131	1.312	C25-C26-C27	119.0912	119.66	N16-N17-C19-O20	-176.004	-175.61
C45-H49	1.0804	0.950	C25-C26-O31	124.973	124.74	N16-N17-C19-N21	4.6533	4.37
N46-C47	1.3753	1.354	C27-C26-O31	115.9358	115.60	H18-N17-C19-O20	-8.8427	-1.16
C47-C48	1.3713	1.341	C26-C27-C28	120.2394	120.16	H18-N17-C19-N21	171.8147	178.82
C47-H50	1.0789	0.950	C26-C27-H36	118.8928	119.92	N17-C19-N21-H22	-2.7691	-1.41
C48-H51	1.0779	0.950	C28-C27-H36	120.8678	119.92	N17-C19-N21-C23	178.6681	-178.05

Table 4. Selected donor-acceptor interactions results of the title compound based on second-order perturbation theory in Fock matrix.

Donor (i)	ED (i) ^e	Acceptor (i)	ED (j) ^e	E(2) ^a (kcal/mol)	E(j)-E(i) ^b (a.u.)	F(i,j) ^c (a.u.)
π C2 - C3	1.68826	π^* C4-C5	0.38017	19.02	0.30	0.069
π C2 - C3	1.68826	π^* C6-C7	0.34163	19.43	0.30	0.069
π C4 - C5	1.68925	π^* C2-C3	0.36664	17.75	0.28	0.064
π C4 - C5	1.68925	π^* C6-C7	0.34163	17.02	0.28	0.062
π C4 - C5	1.68925	π^* C15-N16	0.23453	15.63	0.27	0.059
π C6 - C7	1.70539	π^* C2-C3	0.36664	19.90	0.29	0.070
π C6 - C7	1.70539	π^* C4-C5	0.38017	18.03	0.30	0.067
σ C2 - C3	1.97482	σ^* C2-C7	0.03933	14.47	1.27	0.068
σ C2 - C3	1.97482	σ^* C3-C4	0.01177	12.51	1.29	0.051
π C23 - C24	1.66396	π^* C25-C26	0.39083	18.36	0.28	0.065
π C25 - C26	1.67132	π^* C23-C24	0.38080	20.47	0.29	0.070
π C27 - C28	1.73229	π^* C23-C24	0.38080	17.94	0.29	0.066
π C27 - C28	1.73229	π^* C25-C26	0.39083	18.93	0.29	0.068
π C47 - C48	1.85707	π^* C45-N46	0.37848	15.10	0.28	0.061
LP (2) O1	1.85282	π^* C2-C3	0.36664	26.94	0.35	0.092
LP (2) O8	1.85920	π^* C6-C7	0.34163	26.03	0.36	0.091
LP (1) N16	1.91031	σ^* C15-C38	0.03546	10.80	0.78	0.083
LP (1) N17	1.70419	π^* C15-N16	0.23453	31.90	0.29	0.087
LP (2) O20	1.84694	σ^* N17-C19	0.08098	25.28	0.64	0.116
LP (2) O20	1.84694	σ^* C19-N21	0.07040	23.08	0.71	0.117
LP (1) O20	1.97871	σ^* C24-H29	0.01421	10.53	1.17	0.022
LP (1) N21	1.68358	π^* C23-C24	0.38080	32.67	0.30	0.090
LP (2) O31	1.84921	π^* C25-C26	0.39083	28.52	0.34	0.094
LP (2) O31	1.84921	σ^* C32-H33	0.01950	10.71	0.69	0.058
LP (1) N44	1.56078	π^* C45-N46	0.37848	45.67	0.28	0.102

Table 5. Vibrational assignments of the title compound based on potential energy distribution analysis.

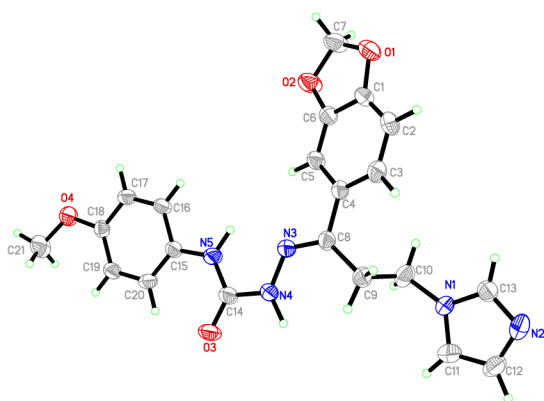
Calculated wavenumbers (cm ⁻¹)	Experimental wavenumbers (cm ⁻¹)		Assignment with PED (%)
	IR	Raman	
3462	3451 vw	-	v N21-H22 (99) Amide
3399	3381 s	-	v N17-H18
3325	3316 w	-	v N21-H22
3203	3197 s	-	v N17-H18
3132	3132 m	-	v C48-H51 (24),C47-H50 (75)
3090	3078 m	3079 m	v C27-H36 (95)
2998	3001 m		v41C-43H (92)
2960	2963 m	2964 m	v _{as} CH ₂ (92) MeI (42)
2944	2936 m		v _{as} CH ₂ (91) MeII (88)
2903	2894 m	2902 w	vC38-H39 (88)
1664	1660 vs	1667 w	v C19=O20 (77)
1604	1609 s	1618 s	v C27-C28 (33)
1580	-	1580 vs	v N16-C15 (33)
1519	1519 vs	1509 m	v C19-N21 (14)
1441	1436 vs	1438 s	d H42-C41-H43 (53)
1398	-	1395 w	β H29-C24-C25 (10)
1346	-	1351 w	W H42-C41-H43 (48)
1339	1338 s		β H50-C47-C48 (10)
1311	1304 s		β C23-C28 (10),C23-C24 (17),C25-C26 (12)
1288		1287 w	d H29-C24-C25 (12),H30-C25-C26 (10)
1267	1277 s		β H50-C47-C48 (25),H51-C48-C47 (13)
1240	1242 vs		d H40-C38-C15-C5 (17)
1175	1179 s	1179 w	v _R H13-C9-O8 (74)
1129	1135 s	1134 w	ρ -OCH ₃ (83)
1103	1102 s	-	β C9-O1-O8-H13 (76),H37-C28-C27 (16),H36-C27-C28(25)
1032	1038 vs	1044 w	W H39-C38-H40 (39)
994	997 m	-	γ C23-C28 (20),C24-C25-C26 (10)

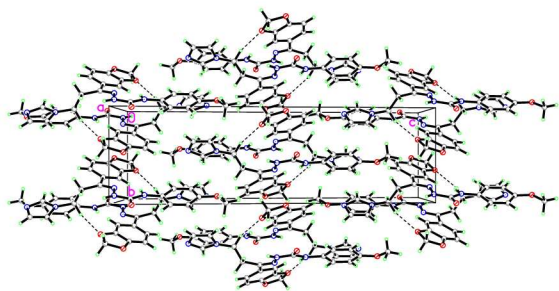
933	947 m	-	Υ C24-C23-C25-H29 (56),H30-C25-C26-O31 (20),H36-C27-C28-H37 (12)
916	920 w	-	Υ C7-C2-O1 (67)
882		875 w	Υ C3-C4-C5 (22)
853	858 w	-	ν C19-N21 (15),N21-C23 (13),C23-C24 (17)
838	827 m	-	Υ H51-C48-C47-N46 (11),C47-C48-N46-H50 (81)
804		807 w	Υ O1-C2-C3 (14)
800	800 m	-	Υ C2-C7-C6 (20)
749	750 m	-	ρ H39-C38-C15-C5 (11), H42-C41-N44-C45 (19)
668	664 m	-	δ N17-C19=O20 (14)
615	619 w	-	Υ N44-C48-C47-N46 (54)
585	591 m	-	τ C25-C26-C27 (12),C5-C15-N16 (10)
509	512 w	-	τ C24-C25-C26-C27 (55),C28-C27-C26-O31 (20)
454	464 vw	-	δ C3-C2-C7 (16),N17-C19-O20 (12)

ν – stretching, ν_{as} -asymmetric stretching, ν_R –ring stretching, β – in plane bending, W – wagging, d – deformation, ρ – rocking, δ – bending, Υ – out of plane bending, τ – torsion, Me I- methylene I, Me II - methylene II, , vs- very strong, s- strong, m- medium, w- weak, vw- very weak.

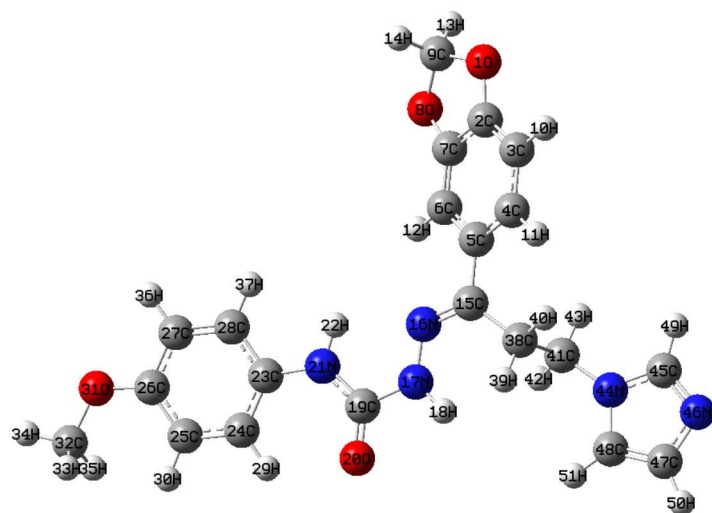
Table 6. Antifungal activity of the title compound towards *C. albicans*, *C. tropicalis*, *C. parapsilosis* and *A. niger*.

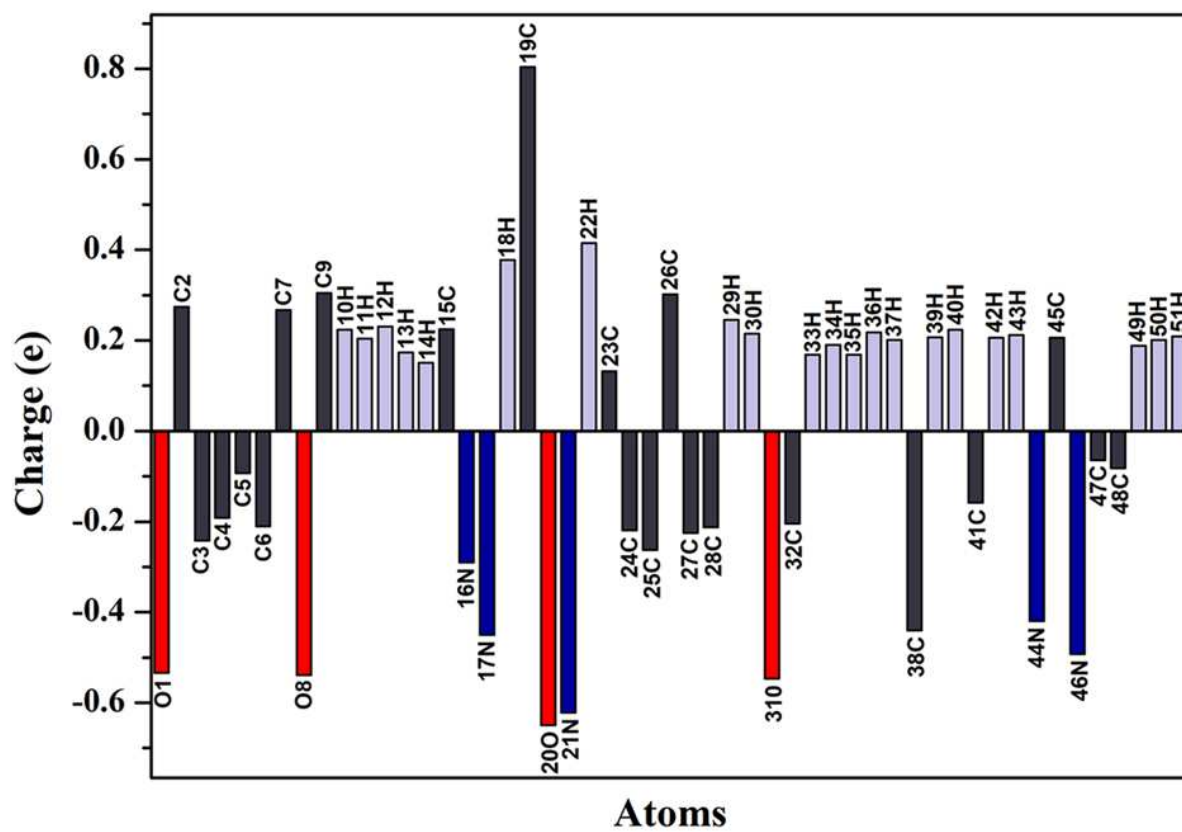
Compound No.	MIC ($\mu\text{mol/mL}$)			
	<i>Candida albicans</i>	<i>Candida tropicalis</i>	<i>Candida parapsilosis</i>	<i>Asperagillus niger</i>
4	0.628	0.314	0.628	0.628
Fluconazole	0.051	0.045	0.047	ND
Ketoconazole	ND	ND	ND	0.02

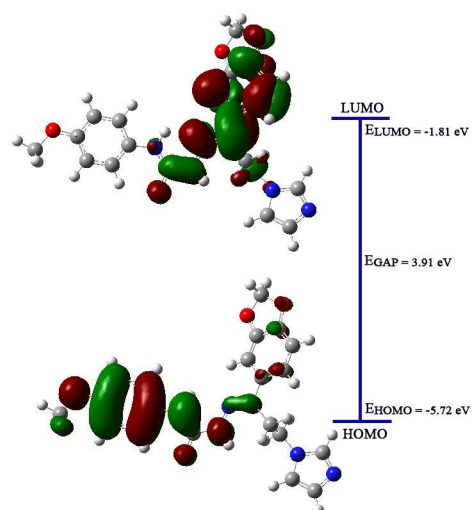




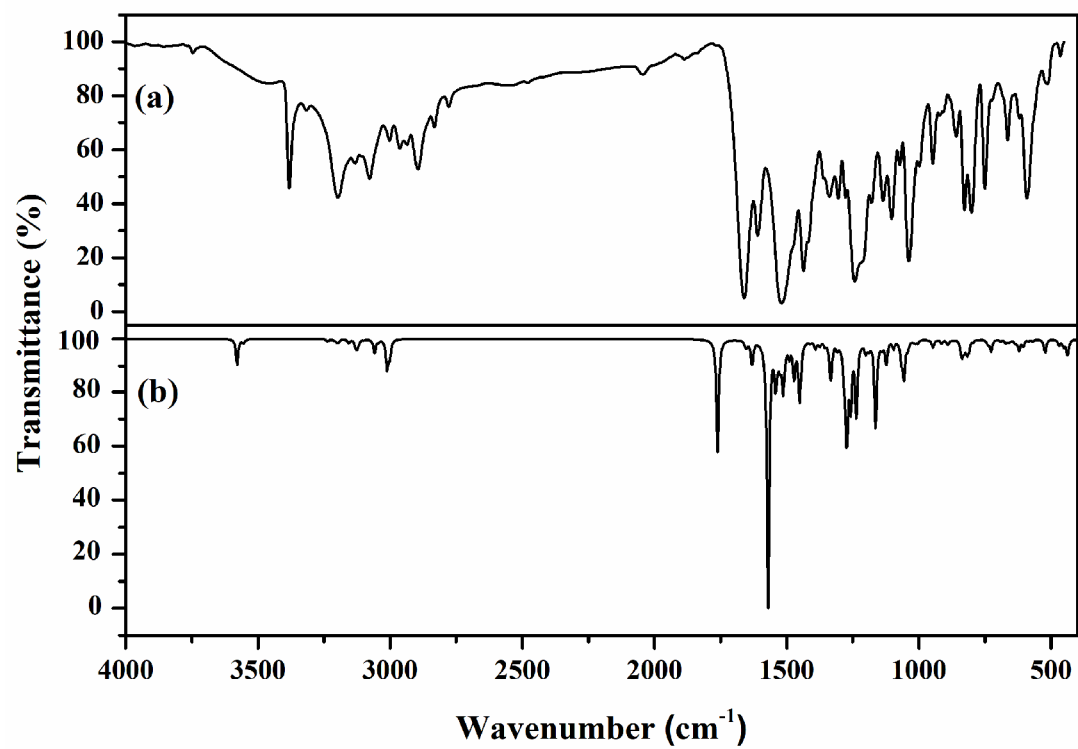
ACCEPTED MANUSCRIPT

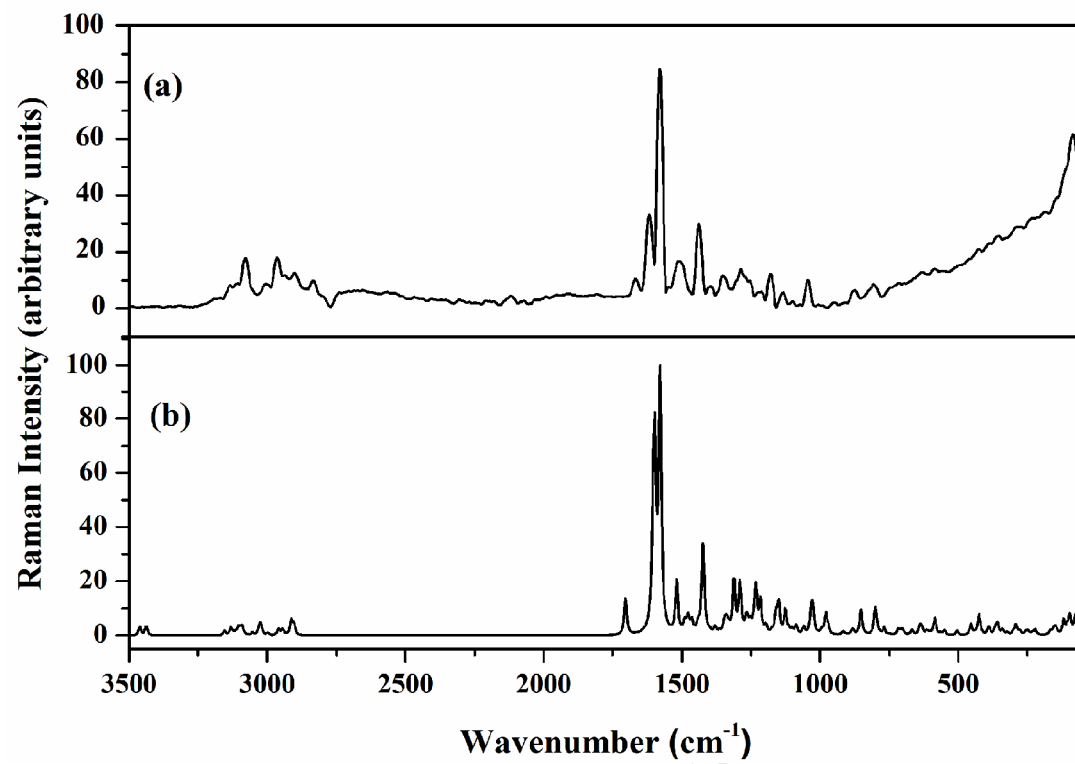


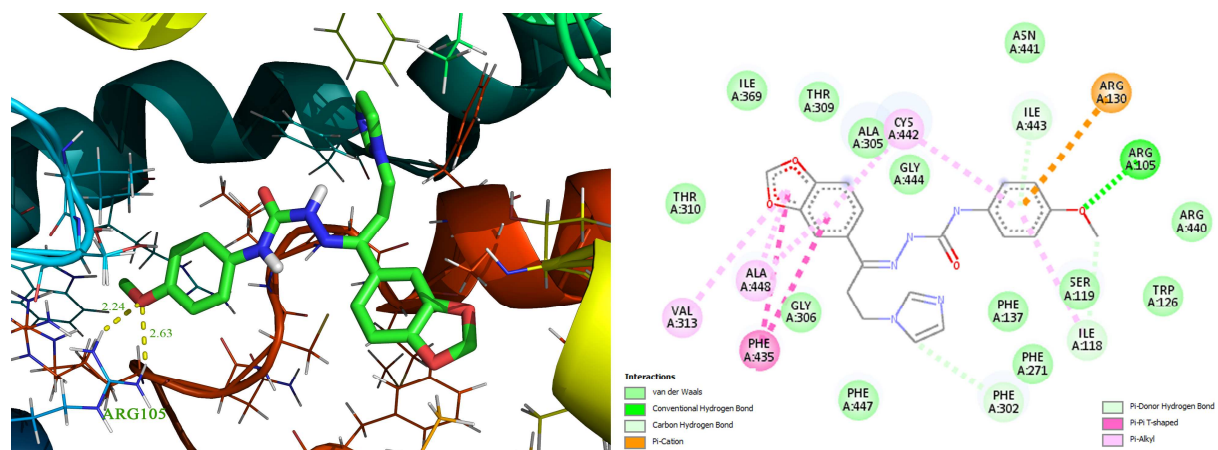




ACCEPTED MANUSCRIPT







- Spectroscopic characterization of a new antifungal agent
- FT-IR, FT-Raman, ^1H and ^{13}C NMR spectral analyses are reported.
- The geometrical parameters are in agreement with the XRD data.
- Molecular docking and antifungal screening were carried out

ACCEPTED MANUSCRIPT